Angewandte Chemie International Edition

Angewandte International Edition Chemie

GDCh German Chemical Society

How to cite: *Angew. Chem. Int. Ed.* **2026**, 65, e22687
doi.org/10.1002/anie.202522687

RESEARCH ARTICLE OPEN ACCESS Hot Paper

Two-Dimensional Polymers as Modular Metal-Free Solid-State Catalysts for Efficient Sono-Piezo-Photocatalytic Hydrogen Peroxide Production

Sarah Brettschneider[1] | Keanu V. A. Birkelbach[1,2] | Marcus Lantzius-Beninga[1,3] | Ahmed Mourran[3] | Gurudas Chakraborty[3] | Peter J. C. Hausoul[1] | Andreas Herrmann[1,3] | Regina Palkovits[1,2,4]

[1]Institute for Technical and Macromolecular Chemistry, RWTH Aachen University, Aachen, Germany | [2]Institute for a Sustainable Hydrogen Economy, Forschungszentrum Jülich GmbH, Jülich, Germany | [3]DWI – Leibniz-Institute for Interactive Materials, Aachen, Germany | [4]Max-Planck-Institute for Chemical Energy Conversion, Mülheim an der Ruhr, Germany

Correspondence: Regina Palkovits (palkovits@itmc.rwth-aachen.de)

Received: 16 October 2025 | **Revised:** 15 January 2026 | **Accepted:** 16 February 2026

Keywords: solid molecular catalysts (SMCs) | piezo-photocatalysis | ultrasound | hydrogen peroxide

ABSTRACT

Piezo-photocatalysis synergistically integrates the features of piezocatalysis and photocatalysis, offering promising applications in environmental remediation, energy conversion, and biomedical therapy. Herein, we introduce modularly designed solid molecular catalysts (SMCs) comprised of metal-free, polyaromatic, two-dimensional polymers which offer an unprecedented level of control over piezopolarization—and consequently, piezo-photocatalysis—through the rational design of structural motifs (diphenylpyridine or terpyridine) and backbone functionalities (methyl group, aliphatic amine antenna, or aromatic pyrrole ring). We demonstrate that piezopolarization, induced by ultrasound across a wide frequency range (35 kHz to 2.6 MHz), enables highly efficient sono-piezo-photocatalytic hydrogen peroxide production. The SMC AP5 featuring the terpyridine motif and pyrrole functionalization is the most active metal-free piezo-photocatalyst for hydrogen peroxide production under ambient conditions. Furthermore, the instantaneous on/off-switchability of the sono-piezo-photocatalysts is shown, underscoring their potential for applications requiring spatiotemporal control over catalytic activity.

1 | Introduction

To achieve a carbon-neutral and sustainable future, cost-effective, safe, and environmentally friendly chemical processes are essential [1, 2]. Conventional methods for hydrogen peroxide (H_2O_2) production—such as the anthraquinone process or electrochemical routes—are often carbon-intensive and energy-demanding [3]. In contrast, polymeric catalysts offer a promising path toward green H_2O_2 production through approaches like photocatalysis or piezo-photocatalysis [4, 5]. As a result, current research focuses on developing catalytic systems that efficiently drive peroxide production under ambient conditions, thereby minimizing the environmental burden from wastewater, exhaust gases, and solid inorganic waste associated with traditional H_2O_2 manufacturing [6–8].

Piezo-photocatalysis represents a sustainable strategy for H_2O_2 production by harnessing renewable energy, such as sunlight, with improved efficiency [9–12]. In line with green chemistry principles, this approach promotes the development of

Sarah Brettschneider and Keanu V.A. Birkelbach contributed equally to this work.

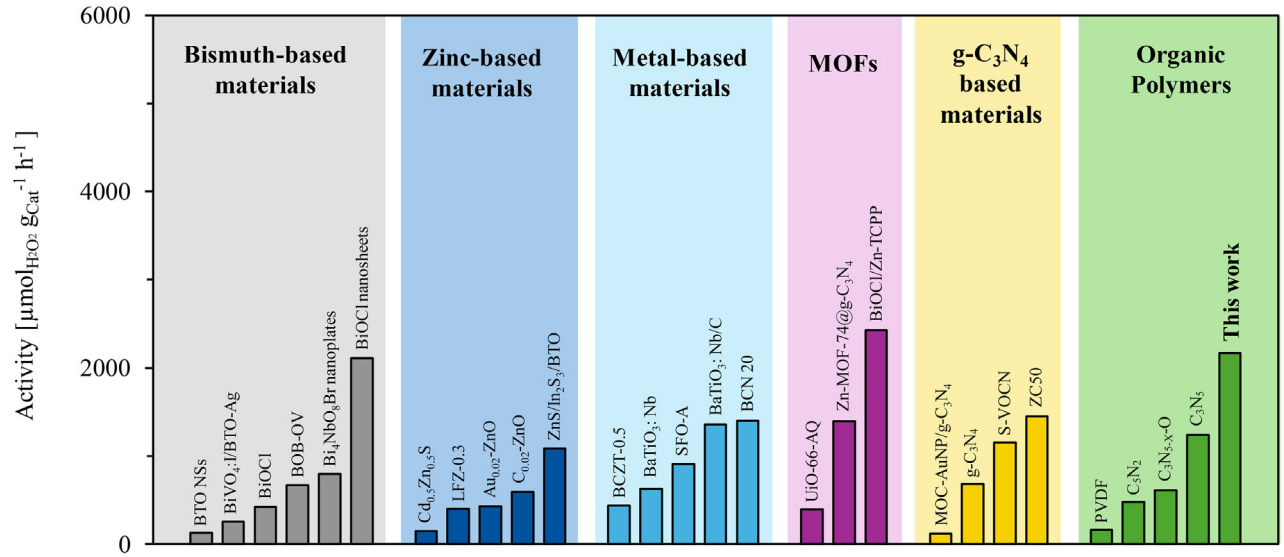

FIGURE 1 | Comparison of different piezo-photocatalysts for H_2O_2 production. The figure illustrates representative material classes, including metal oxides, perovskites, MOFs, g-C_3N_4 derivatives, and organic polymers, highlighting their relative performance. Detailed information about the different systems and the reaction conditions are provided in Table 2 of the Supporting Information.

environmentally friendly technologies [13–15]. While the exact nature of the underlying mechanism remains object of discussion [16], piezo-photocatalysis combines the piezo-electric effect with photocatalysis, wherein mechanical stress generates a piezoelectric polarization within the catalyst material that induces an internal electric field (piezo-potential) [10, 12, 17]. This internal field directs photoinduced electrons and holes in opposite directions, effectively suppressing their recombination — a major limitation in conventional photocatalysis. Consequently, the synergistic piezo–photo activation enhances charge separation and improves photocatalytic efficiency, rendering piezo-photocatalysts superior to their purely photocatalytic counterparts [12, 17, 18].

Over the past decade, piezo-photocatalytic research has primarily focused on water purification [19, 20], water splitting [21, 22], nitrogen fixation [23, 24], carbon dioxide reduction [25, 26], H_2O_2 production [27, 28], and various organic transformations [29–32]. These reactions have been demonstrated mostly at laboratory scale under ultrasound irradiation. A key challenge for advancing this technique toward practical application lies in understanding the interaction between ultrasound and piezo-photocatalysts [9, 12, 16, 33]. Recent studies have explored a variety of piezo-photocatalysts for hydrogen peroxide synthesis, including bismuth-based metal oxides [34], zinc oxides [35–37], $XTiO_3$-type perovskites [38, 39], metal-organic frameworks [40], and metal-doped graphitic carbon nitride [41, 42] (Figure 1). Still, even while not normalizing for varying reaction conditions, only the most active recent catalysts surpass activities of 2000 μmol_{H2O2} g_{Cat}^{-1} h^{-1}, often times necessitating the use of sacrificial agents, enriched atmospheres or harsher conditions [10, 12, 43–46]. Furthermore, organic polymers remain underexplored as catalyst class, even though their flexible choice of different monomers offers opportunities for rational structural tuning and functional optimization [12, 47–49].

Graphitic carbon nitride (g-C_3N_4), a representative nitrogen-containing organic polymer is among the most extensively studied materials for the piezo-photocatalytic production of H_2O_2, owing to its excellent chemical and thermal stability as well as its suitable band structure [41]. Depending on the synthesis route and the morphology of the g-C_3N_4, activities between 57 and 89 μmol_{H2O2} g_{Cat}^{-1} h^{-1} have been reported under ambient conditions [41, 50, 51]. Another widely investigated organic polymer is polyvinylidene fluoride (PVDF), which shows high chemical stability and mechanical flexibility. However, only its β-phase exhibits significant piezocatalytic activity with reported H_2O_2 production rates reaching up to 163 μmol_{H2O2} g_{Cat}^{-1} h^{-1} [47, 52, 53].

Regarding piezo-photocatalysis, one of the most promising subsets of organic polymers are conjugated microporous polymers (CMPs) based on their advantageous material properties. If a CMP exhibits a molecularly defined active site, they are often referred to as solid molecular catalyst (SMC). SMCs thus commonly comprise polycrystalline, thermally stable networks which combine the molecular precision of homogeneous catalysts with the structural robustness of heterogeneous systems. In our previous study, we demonstrated the potential of two-dimensional (2D) SMCs for the photocatalytic H_2O_2 production, with the most active catalyst achieving a rate of 2.31 $mmol_{H2O2}$ g_{Cat}^{-1} h^{-1} under simulated sunlight at half intensity (50 mW cm^{-2}) [54]. Motivated by their strong photocatalytic performance and inspired by the study of Wang et al. [11], we herein report the unprecedented piezo-photocatalytic properties of these SMCs. Remarkably, all tested SMCs exhibited activity under ultrasound exposure. While most piezo-photocatalytic research to date has focused on the degradation of organic pollutants, our objective was to develop a sustainable strategy for H_2O_2 production from water and molecular oxygen under ambient conditions — without the use of metals, additives, UV light, pure oxygen or pressurized conditions [10, 55–57]. Herein, we report a series of modular, air-stable, metal-free SMCs with molecularly defined architectures that enable efficient piezo-photocatalytic H_2O_2 production. The modularity of the SMCs additionally allows the proposal of structure-activity relationships. The most active catalyst in this series exhibits the highest H_2O_2 production rate reported to date for a metal-free system under ambient conditions.

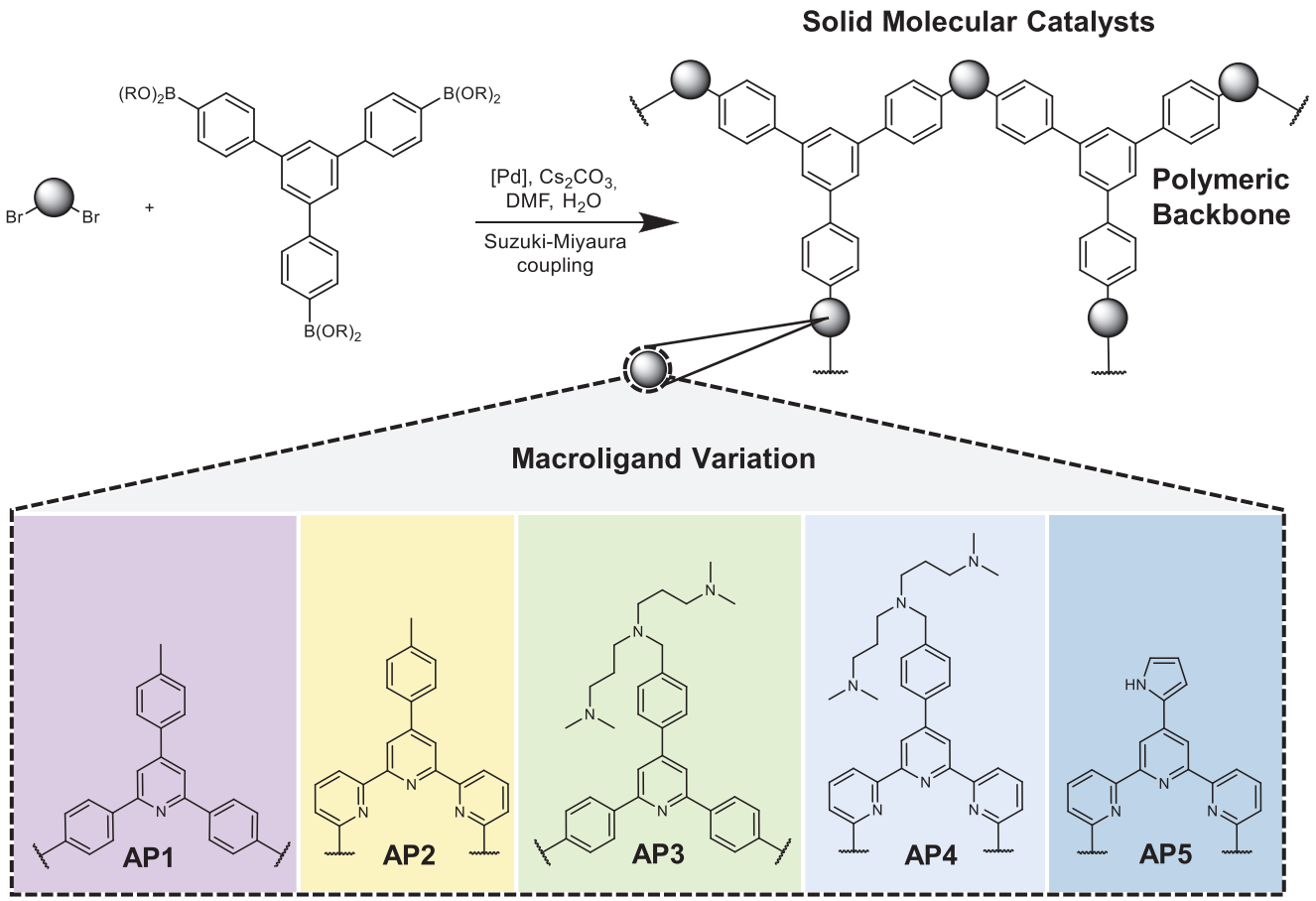

FIGURE 2 | Synthesis and structure of SMCs AP1 to AP5.

2 | Results and Discussion

2.1 | Synthesis and Characterization of SMCs

To elucidate the influence of different structural motifs and backbone functionalities on the piezo-photocatalytic H_2O_2 production, a series of five SMCs, designated as AP1 through AP5 (Figure 2), was synthesized. Structurally, AP1 and AP3 are comprised of a diphenylpyridine motif, whereas a terpyridine motif was incorporated in AP2, AP4, and AP5. Each SMC additionally contains a backbone functionalization. In this regard, AP1 and AP2 both feature a methyl group to allow for a comparison between the diphenylpyridine and terpyridine motif. AP3 and AP4 contain a large, aliphatic amine functionalization, aimed at significantly increasing the hydrophilicity of the SMCs. AP5 incorporates an aromatic pyrrole ring directly attached to the terpyridine structure, adding an additional heterocycle to the conjugated system and altering its electronic makeup.

The SMCs AP1-5 were synthesized based on an amended, previously reported synthetic procedure [54]. The C_3-linker was synthesized following the established procedure described by Wang et al., [58]. The corresponding monomer was synthesized as outlined by Tabrizian et al. and tailored by our group [59].

Solid-state magic angle spinning nuclear magnetic resonance (SS-MAS-NMR) spectra were recorded to confirm the successful formation of the target structures (Figures 3a, S9–S14). The ^{13}C-MAS-SS-NMR spectra of polymers with a diphenylpyridine motif exhibit four peaks within the aromatic region, at 122, 133, 146, and 163 ppm, respectively. The polymers with terpyridine motifs show four peaks within the aromatic region due to the electron withdrawing effect of the nitrogen in the pyridine rings (125, 133, 145, and 161 ppm). Furthermore, for AP3 and AP4, the aliphatic carbons of the backbone antenna can be observed at around 50 ppm. AP5, featuring a pyrrole structure, exhibits two additional signals in the aromatic range (110 and 147 ppm), in agreement with the proposed structure. X-ray photoelectron spectroscopy (XPS) measurements were carried out for further structural verification (Figure 3b,c). High-resolution Br 3d spectra display only residual peaks, indicating successful polymerization, and nearly complete endcapping (see Figure S34). The DRIFTS data further corroborate the successful polymerization, as no bands attributable to B-O stretching vibrations (~1330 cm^{-1}) are detected in the polymer spectra (see Figure S14–S17). To remove potential Pd impurities stemming from the polymerization, all SMCs were stirred in a mixture of hydrochloric acid, H_2O_2 and water and subsequently Soxhlet extracted [57]. The XPS Survey Scan (Figure 3b) showed no residual palladium in the SMCs. High-resolution N 1s scan of backbone-functionalized SMCs (Figure 3c) reveal the presence of two distinct nitrogen signals of strongly varying electron densities for AP3 and AP4 (aliphatic amine and pyridine), and two signals of comparable electron densities for AP5 (pyrrole and pyridine), again confirming their proposed structures. Thermogravimetric analysis (TGA) under air atmosphere reveals thermal stability of the polymer backbone

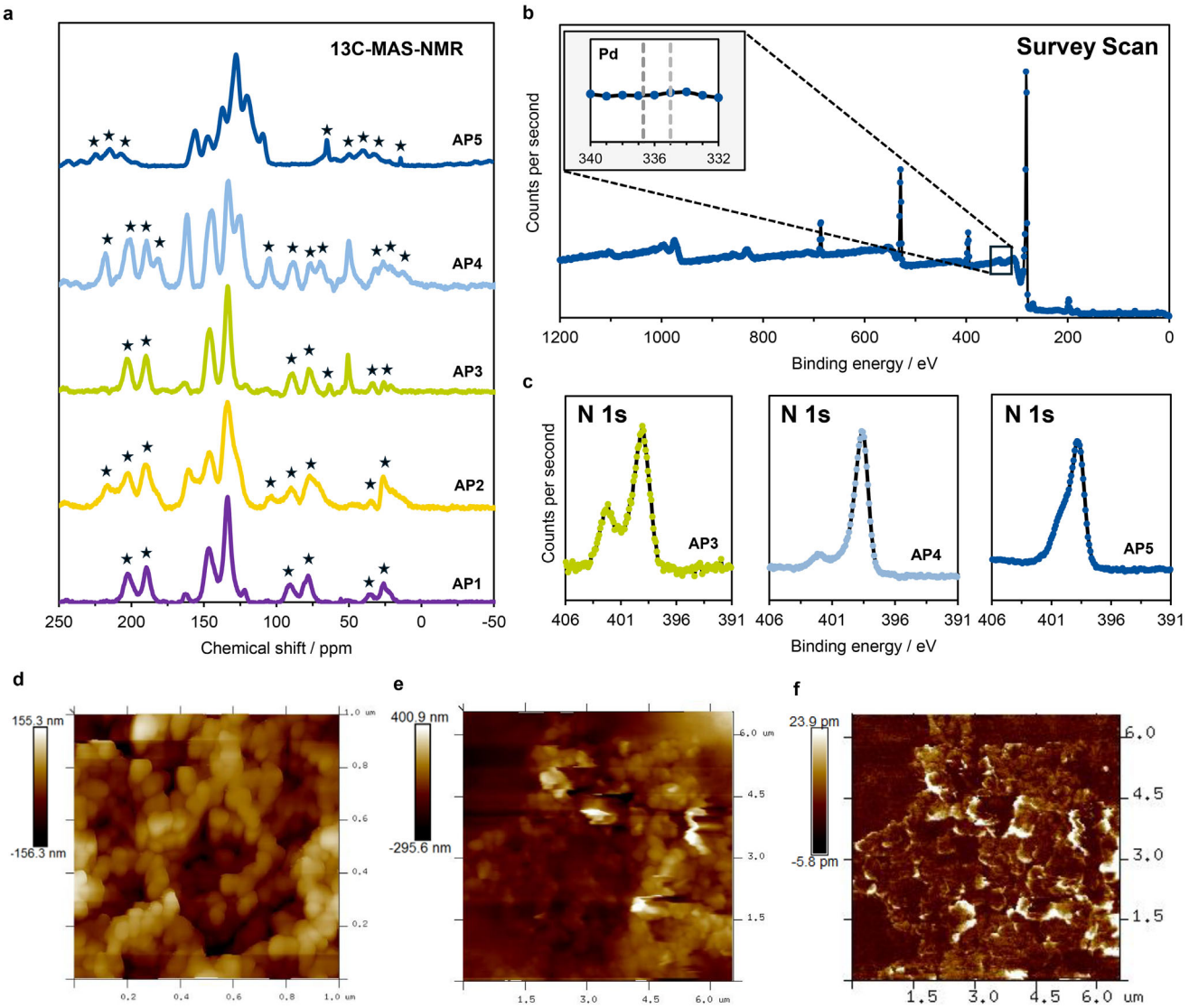

FIGURE 3 | Characterization of SMCs. (a) Solid State 13C-MAS-CC-NMR Spectra. *Spinning side bands. Detailed analysis can be found in the Supporting Information. (b) XPS Survey scan. (c) XPS N 1s high-resolution core-level spectrum. (d) A Tapping-mode AFM height image of AP5 powder shows a sub-100 nm structure when utilizing a tip with a radius of less than 5 nm. (e, f) PFM images of AP5 acquired with a conductive tip (radius < 40 nm), (e) topography image and (f) corresponding piezoresponse amplitude.

up to 450°C (Figure S15), while the amine functionalization in AP3 and AP4 slowly decomposes at temperatures above 180°C. Scanning electron microscopy (SEM) shows large aggregates with irregular edges and abundant holes (Figure S16). In addition, the samples were subjected to x-ray diffraction analysis to determine the extent of crystallinity present in the materials. The diffractograms (Figure S17) show broad reflexes in a regular manner, indicating the polycrystalline structure of the SMC. Additionally, Atomic Force Microscopy (AFM) images (Figure S18) were acquired. The topography image shown in Figure 3d and the phase image presented in Figure S19 both reveal aggregates composed of particles smaller than 100 nm. Moreover, the AFM analysis uncovered a layered structure at the edges of these aggregates, with step heights ranging from 2 to 5 nm. Lastly, to verify the piezoelectric response of these amine-based SMCs, Piezoresponse Force Microscopy (PFM) measurements were performed. For this purpose, a conductive ultrasonic tip was employed, and a single grain of the material was isolated and subsequently pressed onto a conductive aluminum substrate. The conductive tip was modulated with 5 V and a frequency of 15 kHz, while the substrate potential was maintained at 5 V. Figure 3e presents the corresponding topography image, while the simultaneously acquired amplitude of the piezoelectric response is shown in Figure 3f. These results demonstrate that the SMCs exhibit pronounced, voltage-dependent piezoresponsive behavior. In conclusion, the employed synthesis strategy afforded the target metal-free SMCs with the proposed structures as large polycrystalline 2D polymer particles, which possess distinct piezo-responsivity.

2.2 | Piezo-Photocatalytic Behavior of SMCs

Piezo-photocatalysis combines photocatalysis and piezocatalysis in a synergistic manner, utilizing both light and mechanical energy to drive chemical reactions. The internal electric

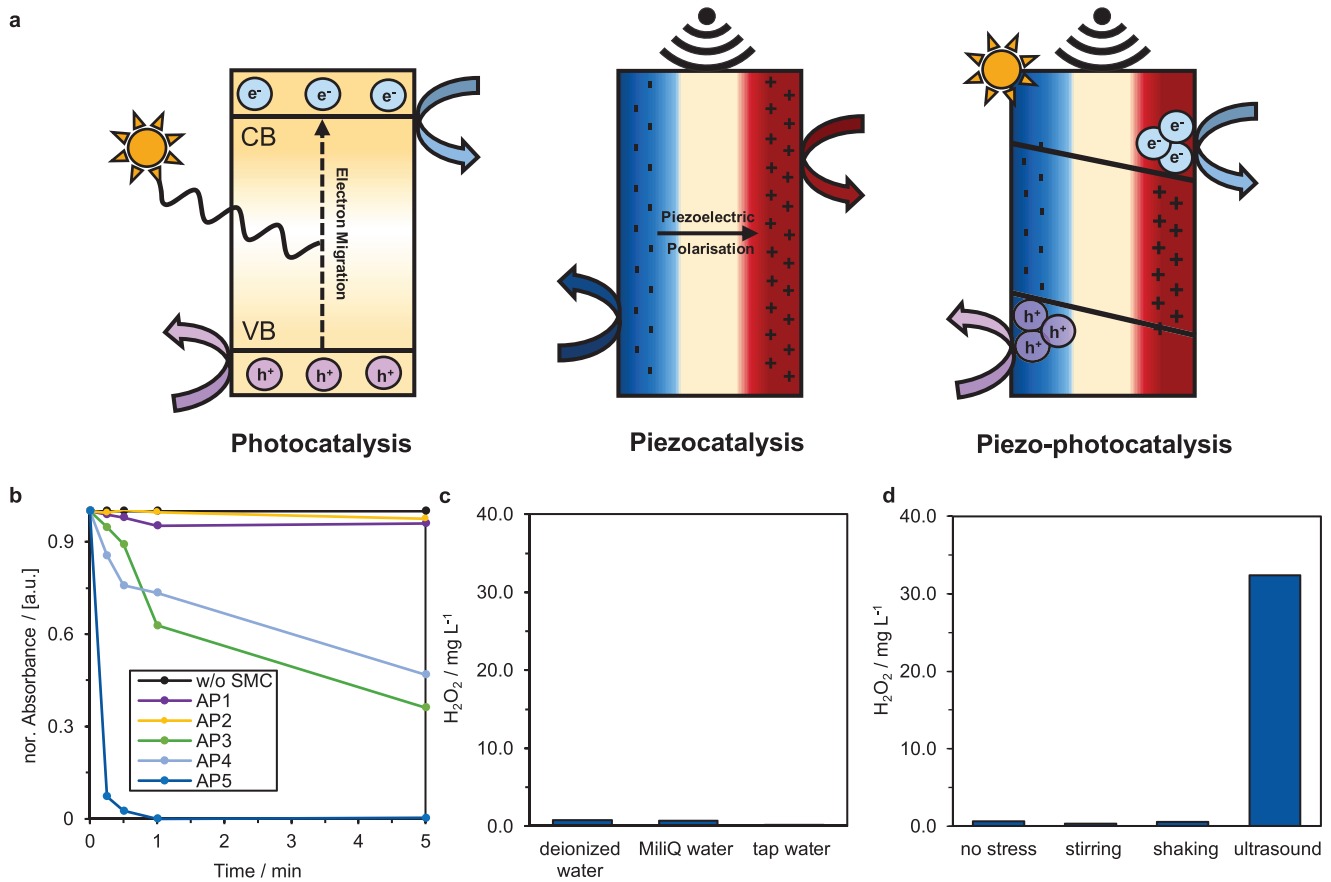

FIGURE 4 | Proof of piezo-Photocatalytic behavior of SMCs. (a) Schematic illustration of the mechanisms of photocatalysis, piezocatalysis, and piezo-photocatalysis (b) Time-resolved absorbance of potassium permanganate (40 mg L^{-1}) at 525 nm under ultrasonic irradiation with and without SMC AP5 (3 mg, 6 mL solution, 45 kHz ultrasonic bath, ambient conditions). (c) Influence of different ion concentrations on the production of H_2O_2 (6 mL water, 45 kHz, 1 h). (d) Influence of the type of mechanical stress on the piezo-photocatalytic activity (3 mg AP5, 6 mL water, stirring at 1000 rpm or shaking bath with 100 rpm orultrasonic bath with a frequency of 45 kHz, 1 h).

field generated by the piezoelectric effect enhances the separation of photogenerated charge carriers, leading to significantly improved catalytic efficiency compared to either process alone (Figure 4a) [12, 60]. In order to verify that the multi-energy piezo-photocatalysis is the underlying mechanism when employing the presented SMCs, a series of preliminary reactions was carried out. The piezo-photocatalytic activity of the SMCs was tested using an established procedure [11]. To this end, potassium permanganate ($KMnO_4$) was reduced by piezo-photocatalytically generated electrons [11]. The reduction of $KMnO_4$ was monitored via UV Vis spectroscopy based on the absorbance at around 525 nm (Figure 4b) [11].

In the absence of SMCs, the absorbance of the $KMnO_4$ solution exposed to ultrasound at ambient light did not change, confirming its stability in the presence of such ultrasonic irradiation (Figure 4b). In comparison, in the presence of either of the five different SMCs the time-resolved reduction of $KMnO_4$can be observed upon ultrasonication. The methyl-functionalized AP1 and AP2 show the lowest decomposition activities within 5 min. The differently functionalized SMCs show higher activity increasing from AP4 to AP3 to AP5. For AP5, no absorbance remained at 525 nm after 5 min of ultrasonic irradiation, evidencing the complete reduction of $KMnO_4$ and in turn its exceptional piezo-photocatalytic activity. In sonocatalysis, reactive oxygen species (ROS) are generated through the reaction of oxygen with charge carriers, especially electrons (e^-) and electron holes (h^+), at the catalyst surface. The four major ROS are superoxide anion radicals, singlet oxygen, hydroxy radicals, and H_2O_2 [2, 47, 61, 62]. To rule out a contribution of metal impurities in the employed water to the observed overall activity, different purity levels of water were sonicated. In these experiments, the concentration of catalytically produced hydrogen peroxide was used to determine activity since its quantification is possible using colorimetric methods. Figure 4c shows that such produced H_2O_2 is negligible in the absence of a catalyst and no major difference between the various purity levels of water and ion concentrations was observed. Lastly, the impact of the nature of the induced mechanical force was investigated. In the absence of mechanical force, a concentration of 0.64 mg L^{-1} H_2O_2 was measured, which corresponds to the purely photocatalytic activity of the SMC. In this study, three different forms of mechanical input were investigated: stirring, shaking, and ultrasound. For stirring and shaking, frictional energy serves as the driving force (tribocatalysis), whereas under ultrasonic conditions, the primary excitation source is the ultrasonic energy (piezo-/sonocatalysis) [63]. Stirring or shaking of the reaction mixture did not lead to a significant increase in H_2O_2 concentration, while

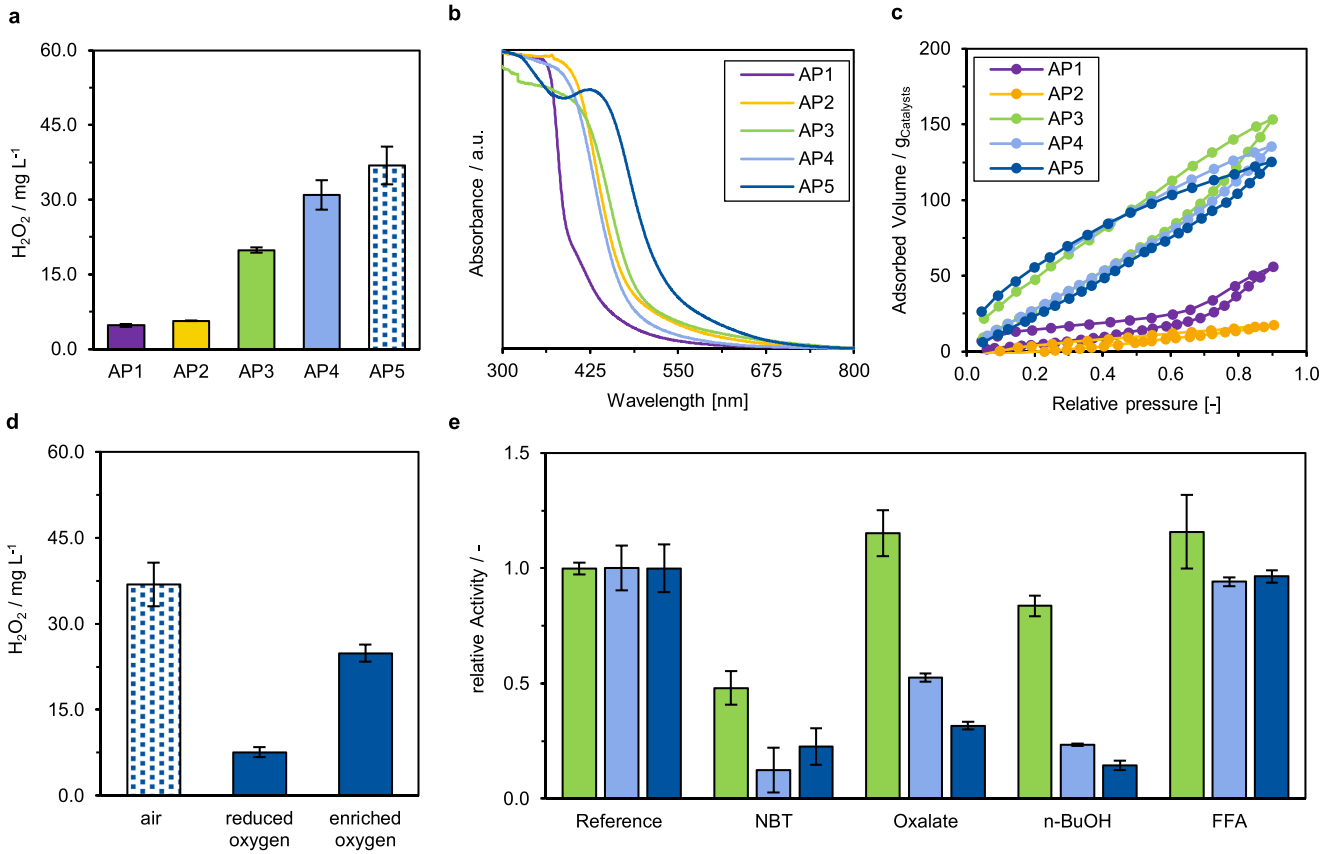

FIGURE 5 | Piezo-photocatalytic production of H_2O_2 from water and oxygen. (a) Comparison of the activity of five SMCs (0.5 mg/mL) with different motifs and backbone functionalities at 45 kHz. (b) Solid UV/Vis spectra of the investigated SMCs. (c) Water physisorption isotherms of the SMCs. (d) Influence of reduced (0.2 mg L^{-1}) and enriched (> 20 mg L^{-1}) oxygen atmosphere on the piezo-photocatalytic performance of AP5 (3 mg AP5, 6 mL water, 45 kHz, 1 h). (e) Radical scavenger experiments (0.05 mM solution, 3 mg AP5, 6 mL water, 45 kHz, 1 h). The dotted markers indicate measurements from the reference experiment. Error bars represent standard deviation from $N \geq 2$ independent measurements.

ultrasound irradiation resulted in a peroxide concentration of 32.4 mg L^{-1}. Collectively, these findings indicate that frictional energy alone is insufficient to activate the catalyst, confirming that the observed catalytic activity arises from a combined piezo-/sono-photocatalytic mechanism.

2.3 | Piezo-Photocatalytic H_2O_2 Production

In order to quantify the piezo-photocatalytic activity of the SMC series, the production of H_2O_2 was again used as a model reaction. In an initial series of experiments, all SMCs were screened under uniform conditions to identify the influence of their individual structural inclusions on catalytic activity (Figure 5a).

AP1 and AP2, featuring a methyl functionalization along the diphenylpyridine or terpyridine structure, respectively, showed the lowest catalytic activities in the series, resulting in peroxide concentrations below 7 mg L^{-1}. Between the two, the reaction employing AP2, based on the terpyridine structure, exhibited a minimally higher peroxide concentration. Upon inclusion of the large aliphatic amine functionalization, both the diphenylpyridine- (AP3) and terpyridine-based (AP4) SMC exhibited significantly increased peroxide production rates. Additionally, the gap in activity between the two aromatic backbone types widened substantially, with AP3 resulting in a peroxide concentration of around 20 mg L^{-1}, while AP3 achieved a concentration of around 30 mg L^{-1}. Based on this, it can be concluded that the terpyridine scaffold is superior to the phenylpyridine one in the context of the piezo-photocatalytic production of H_2O_2. Furthermore, the addition of the aliphatic amine motif significantly improved the catalytic activity of both scaffold types, evidencing that an increased hydrophilicity of SMCs benefits catalytic activity, most likely through improved catalyst/solvent, and thus substrate, interaction. Lastly, employing AP5, featuring a pyrrole antenna directly attached to the terpyridine structure in lieu of the aliphatic amine, resulted in the highest peroxide concentration of the series, at 36.9 mg L^{-1}. Despite also increasing the N content of the overall SMC, the pyrrole is expected to increase the hydrophilicity of the material less than the highly basic aliphatic amines of AP3 and AP4, and the observed improved catalytic activity is instead attributed to beneficial changes to the properties of the conjugated, aromatic system. To further substantiate these claims, band gap energy solid state UV/vis spectra (Figure 5b) were recorded via the Tauc method [64–67]. AP1 shows the highest band gap energy in the series with 3.12 eV, whereas AP2 to AP4 show similar band gaps between 2.54 eV to 2.65 eV. The lowest band gap energy is exhibited by AP5 with 2.34 eV. This finding is in agreement with the observed catalytic activity trends and validates the proposed effect of the pyrrole

structure on the properties of the conjugated system as main cause for the exceptional activity of AP5. While the band gap is a significant determinant of the catalytic activity, the hydrophilicity of the SMCs was also proposed as a key differentiator. Figure 5c thus shows water physisorption measurements of all SMCs in the series. As expected, the adsorbed volume and therefore the hydrophilicity increased drastically upon introduction of additional nitrogen-containing functionalities. Interestingly, the pyrrole-functionalized AP5 shows a hydrophilicity comparable to the aliphatic amine-containing AP3 and AP4. With the nitrogen to carbon ratio, the partial charge and therefore polarity of the polymers increased. Furthermore, the adsorbed volume of water per active surface area for a monolayer of water was calculated. The adsorbed volume of water per active surface area increases from AP1 to AP5, AP1 to AP5, with values of 0.131, 0.142, 0.918, 1.253, and 1.975 $cm^3\ m^{-2}$, respectively, correlating with the observed catalytic activity trends (Table S1). Next, reaction parameters were varied to quantify their impact on the catalytic activity of the best-performing AP5. Mechanistically, H_2O_2 can be produced via the oxygen reduction reaction (ORR) or the water oxidation reaction (WOR) [13]. In the reductive mechanism, molecular oxygen can be reduced via a one-, two- or four-electron process. In the one-electron transfer mechanism oxygen is reduced to super oxide radicals, which can be protonated to hydroperoxyl radicals. In a second electron transfer these active oxygen species can be further reduced and protonated to form H_2O_2. In the direct two-electron transfer mechanism, oxygen is directly converted to H_2O_2. Unfortunately, a further reduction of H_2O_2 to water via the four electron pathway is also possible [13, 68, 69]. The ORR commonly represents the main contributor to the overall activity in the catalytic production of H_2O_2. As oxygen is the key reactant of this mechanistic pathway, the influence of the oxygen concentration on the catalytic activity was investigated via experiments with reduced (0.20 mg L^{-1}) or enriched (>20 mg L^{-1}) oxygen content (Figure 5d). The oxygen content of the reaction system was adjusted by flushing argon or pure oxygen through the suspension for ten minutes. Afterwards, the reaction tube was sealed. With reduced oxygen content, catalytic activity decreased by 80%. In Addition, the reaction was repeated in the presence of an increased oxygen content. Surprisingly, the catalytic activity also decreased, albeit by just 30%. In literature, several decomposition mechanisms of H_2O_2 through oxygen radicals, such as Fenton-like reactions or the Haber-Weiss reaction, are known [70, 71]. In the Haber-Weiss decomposition mechanism, superoxide radicals react with H_2O_2 to form oxygen, hydroxyl anions and hydroxy radicals [71]. We propose that with increasing oxygen content the decomposition rate of H_2O_2 via a Haber-Weiss like reaction becomes faster than the production of H_2O_2 resulting in the overall lower concentration. Of the three tested conditions, air atmosphere was thus shown to be the most beneficial. While this is a promising circumstance from an application point of view due to the simplicity of using air, it is likely that the catalytic activity of AP5 could further be improved by varying the oxygen content with a higher degree of control. As an additional angle to uncover the underlying reaction mechanisms, radical scavenging experiments were conducted with the three most active SMCs. Scavengers were chosen to inhibit the stepwise oxygen reduction reaction (NBT, $O_2^{-\cdot}$) the direct and stepwise water oxidation reaction (oxalate, h^+), the isolated stepwise water oxidation reaction (n-BuOH, $OH^\cdot$) and the singulet oxygen pathway (FFA, $^1O_2$). As shown in Figure 5e, in the presence of NBT a significant reduction in catalytic activity was observed for all SMCs, pointing towards the ORR being the major mechanistic pathway towards hydrogen peroxide. The presence of oxolate increased the catalytic activity of AP3 while reducing that of AP4 and AP5. The increased activity with AP3 can be attributed to oxolate acting as a sacrificial agent rather than a scavenger and is thus evidence of the WOR not significantly contributing to the overall activity of that SMC. In contrast, for AP4 and AP5 the presence of oxolate resulted in reduced catalytic activity, suggesting that the WOR is taking place in addition to the ORR for these SMCs. Interestingly, in the presence of n-BuOH, which is supposed to impact the stepwise WOR exclusively, a reduction in catalytic activity was observed for AP3, for which we propose no WOR is taking place. Furthermore, the reduction of catalytic activity for AP4 and AP5 is more pronounced than in the presence of oxolate, which should quench both the direct and indirect WOR pathway. Both findings can, however, be explained when considering the homolytic cleavage of H_2O_2 into two hydroxy radicals. Even if the cleaved peroxide was produced without hydroxy radicals as intermediates, for example via the ORR, its cleavage and the subsequent inhibition of recombination by quenching would result in a reduced overall catalytic activity, matching the observed trends. No impact was found on catalytic activity in the presence of furfuryl alcohol, suggesting that it does not play a role in the piezophotocatalytic production of peroxide. Together, these experiments confirm that in all cases the production of H_2O_2 mainly follows the oxygen reduction mechanism, while for the SMCs containing the terpyridine motif and aliphatic amine functionalization (AP4) or pyrrole functionalization (AP5), the WOR is enabled as an additional mechanistic pathway. Based on this observation, an additional reaction in a closed system was performed to investigate the water splitting ability of the catalyst. However, in the gas sample no hydrogen could be detected, which suggests that the catalysts are not active in water splitting. Next, the effect of the light source on the piezo-photocatalytic reaction was investigated (Figure 6a). Compared to the reference at room light with an intensity between just 3 W m^{-2} and 6 W m^{-2}, under dark conditions (0 W m^{-2}) the activity was 35% lower. The remaining activity can be attributed to the purely piezocatalytic capabilities of the SMC. The pronounced impact of the low intensity room light underlines the synergistic impact of piezo-photocatalysis. Upon additional irradiation of the ultrasound bath with UV Light (365 nm, 1000 W m^{-2}), the H_2O_2 concentration of the product solution increased by 41% up to 52 mol L^{-1}.

These findings highlight the potential for a combined and synergistic approach utilizing piezo- and photocatalysis, as the highest overall yield of H_2O_2 was obtained. At the same time, the catalyst already showed exceptional activity at ambient light with light intensities between just 3 W m^{-2} and 6 W m^{-2}. Since the use of additional UV light also entails a significant increase in the energy demand of the overall setup, and since UV usage carries negative implications regarding catalyst and material stabilities, the ability to maintain a majority of the catalytic activity using ambient light is a key advantage of the presented system over existing piezo-photocatalysts [72, 73]. Lastly, the influence of the ultrasound frequency and intensity was further examined. Typical frequencies used for sonocatalysis start above the audible range (20 kHz) and extent into the megahertz region, whereby the cavitation strength increases with decreasing frequency [74, 75]. To be able to cover this entire frequency range, two set-ups

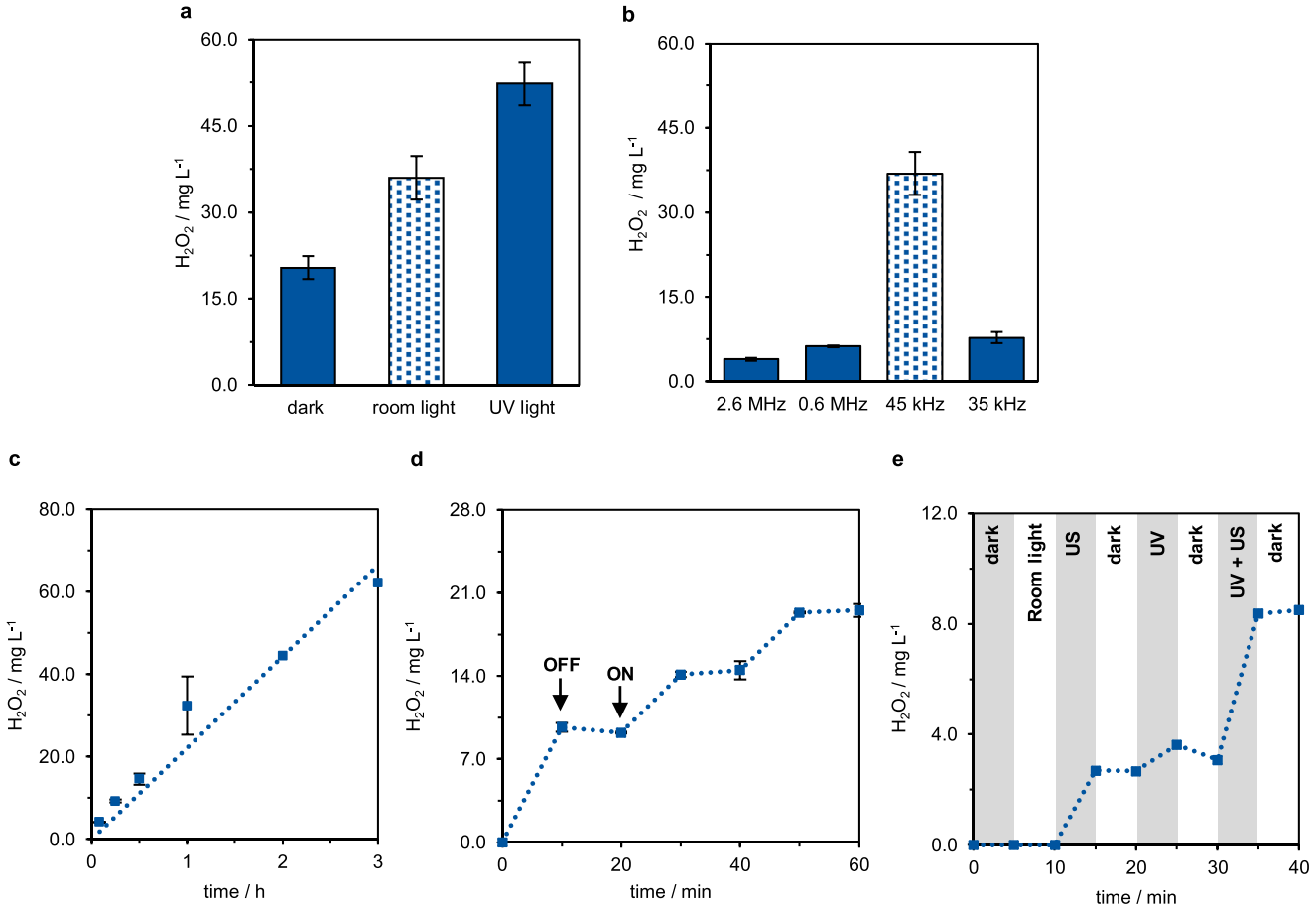

FIGURE 6 | Time-resolved and ON/OFF studies. (a) Influence of light source on the piezo-photocatalytic activity (3 mg AP5, 6 mL water, 45 kHz, 1 h, dark: 0 W m^{-2}, room light: 3 – 6 W m^{-2} and UV light: 365 nm, 1000 W m^{-2}). (b) Influence of the ultrasonic frequency on catalytic activity (3 mg AP5, 6 mL water, 1 h). The dotted markers indicate measurements from the reference experiment. (c) Time-resolved study using AP5 under ambient conditions (3 mg AP5, 6 mL water, 45 kHz, air, room light). (d) ON-OFF-ON experiments of ultrasonic with 45 kHz and AP5 (3 mg AP5, 6 mL water, air, room light). (e) Switching between piezocatalysis, photocatalysis, and piezo-photocatalysis with AP5 (3 mg AP5, 6 mL water, air, 5 min intervals, UV lamp: 365 nm, 500 W/m^2, US: 45 kHz, 120 W) Detailed information about the modified set-up can be found in the Supporting Information. Error bars represent standard deviation from $N \geq 2$ independent measurements.

for sonication were deployed (see Supporting Information). Importantly, the change in frequency can significantly alter the mode of energy input to the reaction. As an example, under standard conditions cavitation no longer takes place at very high frequencies [76–79]. Consequently, a quantitative comparison of catalytic activity is difficult across a wide frequency range, and this set of experiments are instead intended to analyze if catalytic activity remains at a particular frequency, and in turn if the SMC was suitable for an application requiring it.

Figure 6b illustrates that activity remained at all frequencies. The activity of the catalysts increases from 2.6 MHz to the reference experiment at 45 kHz and drops again at lower frequencies. This surmises that the resonance frequency of the material is around 45 kHz. Noteworthily, even though the overall catalytic activity decreased, the presented SMC maintained its ability to be stimulated by biocompatible ultrasound with frequencies above 2 MHz [75]. At 2.6 MHz, for instance, the production of 3.9 mg L^{-1} of H_2O_2 per hour remains possible (Figure 6b). This carries important implications for a potential application of these systems in a medical context [79]. Furthermore, the influence of the ultrasound intensity was tested. With an increasing intensity from 50 % to 100 % at a fixed frequency of 0.6 MHz the catalytic activity steadily increases from 4.6 mg L^{-1} to 6.3 mg L^{-1}. All following experiments were performed with an ultrasound frequency of 45 kHz and 100% intensity. In summary these experiments showed that the presented SMC exhibited the highest efficiency with the simplest reaction set-up: air atmosphere, room light, and an ultrasound bath. Subsequently, in order to achieve even higher peroxide concentrations, an extended reaction employing the best-performing SMC AP5 was carried out for 3 h. As a result, a H_2O_2 concentration exceeding 60 mg L^{-1} was obtained (Figure 6c). The observed linear correlation between reaction time and peroxide concentration (R^2 = 0.98) during the reaction proves both that the catalytic system remained stable throughout this time and that no equilibrium was reached. Additionally, a series of adaptive ON-OFF experiments (Figure 6d) was conducted. As can be seen in Figure 6d, the catalytic production hydrogen peroxide can be precisely controlled via ultrasound. Upon its deactivation, no increases in H_2O_2 levels can be observed. Upon reactivation of ultrasound, the production of peroxide continues in an immediate

and fast manner. This means that both the timing and the concentration of H_2O_2 can be controlled by the applied ultrasonication time, and that the presented SMC is switchable through the application of mechanical force. Furthermore, the possibility of switching between piezocatalysis, photocatalysis, and piezo-photocatalysis was investigated. The corresponding results are presented in Figure 6e, demonstrating that hydrogen peroxide generation occurs under all three activation modes. Moreover, a synergistic effect is observed for piezo-photocatalysis, as the resulting hydrogen peroxide concentration increases significantly compared to the sum of the individual contributions.

3 | Conclusion

In conclusion, five structurally different, modular, metal-free, amine-based SMCs were successfully synthesized and applied in the piezo-photocatalytic production of H_2O_2. Owing to their modular design, it was possible to correlate the incorporation of various functional groups with changes to the band gap energy and the hydrophilicity of the SMCs and ultimately with their observed catalytic activities. Among them, AP5, comprised of a terpyridine structure and a pyrrole functionalization, exhibited the highest performance, achieving a H_2O_2 concentration of 36.9 mg L^{-1} h^{-1} under ultrasound irradiation at 45 kHz in water, using only low-intensity room light and normal atmosphere. As such, these SMCs rank among the most efficient metal-free catalyst systems for the H_2O_2 production under ambient conditions. Furthermore, catalytic activity was maintained even under high-frequency, biocompatible ultrasound (>2 MHz), demonstrating the robustness of the system and showcasing the potential for application in a medical context. In time-dependent and ON-OFF switching experiments, the long-term stability of AP5 was shown, and it was confirmed that H_2O_2 production could be externally regulated by ultrasound, allowing precise control of the timing and extent of peroxide production. In addition, it could be shown, that these materials can switch between piezocatalysis, photocatalysis, and piezo-photocatalysis, which highlights the potential of these systems for controllable, on-demand applications.

Author Contributions

Sarah Brettschneider: writing – original draft, investigation, formal analysis, data curation, conceptualization. **Keanu V.A. Birkelbach**: writing – original draft review & editing, investigation, formal analysis, data curation, conceptualization. **Marcus Lantzius-Beninga**: writing – review & editing, investigation, formal analysis, data curation, validation. **Ahmed Mourran**: writing – review & editing, investigation, formal analysis. **Gurudas Chakraborty**: writing – review & editing, validation, supervision, project administration, methodology, conceptualization. **Peter J.C. Hausoul**: writing – review & editing, validation, supervision, project administration, methodology, conceptualization. **Andreas Herrmann**: writing – review & editing, supervision, resources, project administration, methodology, funding acquisition, conceptualization. **Regina Palkovits**: writing – review & editing, supervision, resources, project administration, methodology, funding acquisition, conceptualization.

Acknowledgments

We acknowledge the Werner Siemens Foundation for funding in the frame of the WSS Research Center *catalaix*—catalysis for a circular economy. S.B. and K.B. thank the Cluster of Excellence Fuel Science Center (EXC 2186, ID: 390919832) by the Excellence Initiative of the German federal and state governments to promote science and research at German universities for funding. This work was supported by the EU through an ERC Advanced Grant (SONOPHARMAGEN, No. 101142296, to A.H.). Moreover, this work was funded as part of the Leibniz ScienceCampus: ACTISONO, supported by the Leibniz Association (No. W89/2023, to A.H.). M.L-B. gratefully acknowledges support from the German Scholarship Foundation for a PhD scholarship. We thank Jan Decker for his work in the lab and Dr. Rostislav Vinokur for his help with HIFU experiments.

Open access funding enabled and organized by Projekt DEAL.

Conflicts of Interest

The authors declare no conflicts of interest.

Data Availability Statement

All raw data generated during this study are available on Zenodo (DOI: https://doi.org/10.5281/zenodo.18850109).

References

1. J. B. Zimmerman, P. T. Anastas, H. C. Erythropel, and W. Leitner, "Designing for a Green Chemistry Future," *Science* 367 (2020): 397.

2. Z.-S. Zhu, S. Zhong, C. Cheng, et al., "Microenvironment Engineering of Heterogeneous Catalysts for Liquid-Phase Environmental Catalysis," *Chemical Reviews* 124 (2024): 11348.

3. S. Siahrostami, S. J. Villegas, A. H. Bagherzadeh Mostaghimi, et al., "A Review on Challenges and Successes in Atomic-Scale Design of Catalysts for Electrochemical Synthesis of Hydrogen Peroxide," *Acs Catalysis* 10 (2020): 7495.

4. C. Hu, S. Tu, N. Tian, T. Ma, Y. Zhang, and H. Huang, "Photocatalysis Enhanced by External Fields," *Angewandte Chemie International Edition* 60 (2021): 16309.

5. F. Chen, H. Huang, L. Guo, Y. Zhang, and T. Ma, "The Role of Polarization in Photocatalysis," *Angewandte Chemie International Edition* 58 (2019): 10061.

6. J. M. Campos-Martin, G. Blanco-Brieva, and J. L. G. Fierro, "Hydrogen Peroxide Synthesis: An Outlook Beyond the Anthraquinone Process," *Angewandte Chemie International Edition* 45 (2006): 6962.

7. Q. Wu, J. Cao, X. Wang, et al., "A Metal-Free Photocatalyst for Highly Efficient Hydrogen Peroxide Photoproduction in Real Seawater," *Nature Communications* 12 (2021): 483.

8. S. Wang, Z. Xie, D. Zhu, et al., "Efficient Photocatalytic Production of Hydrogen Peroxide Using Dispersible and Photoactive Porous Polymers," *Nature Communications* 14 (2023): 6891.

9. J. He, C. Dong, X. Chen, et al., "Review of Piezocatalysis and Piezo-Assisted Photocatalysis in Environmental Engineering," *Crystals* 13 (2023): 1382.

10. S. Tu, Y. Guo, Y. Zhang, et al., "Piezocatalysis and Piezo-Photocatalysis: Catalysts Classification and Modification Strategy, Reaction Mechanism, and Practical Application," *Advanced Functional Materials* 30, no. 48 (2020): 2005158.

11. K. Wang, D. Shao, L. Zhang, Y. Zhou, H. Wang, and W. Wang, "Efficient Piezo-Catalytic Hydrogen Peroxide Production From Water and Oxygen Over Graphitic Carbon Nitride," *Journal of Materials Chemistry A* 7 (2019): 20383.

12. L. Jing, Y. Xu, M. Xie, et al., "Piezo-Photocatalysts in the Field of Energy and Environment: Designs, Applications, and Prospects," *Nano Energy* 112 (2023): 108508.

13. H. Hou, X. Zeng, and X. Zhang, "Production of Hydrogen Peroxide by Photocatalytic Processes," *Angewandte Chemie International Edition* 59 (2020): 17356.

14. A. Chakraborty, A. Alam, U. Pal, et al., "Enhancing Photocatalytic Hydrogen Peroxide Generation by Tuning Hydrazone Linkage Density in Covalent Organic Frameworks," *Nature Communications* 16 (2025): 503.

15. K. N. Ganesh, D. Zhang, S. J. Miller, et al., "Green Chemistry: A Framework for a Sustainable Future," *Organic Process Research & Development* 25 (2021): 1455.

16. K. Wang, C. Han, J. Li, J. Qiu, J. Sunarso, and S. Liu, "The Mechanism of Piezocatalysis: Energy Band Theory or Screening Charge Effect?," *Angewandte Chemie—International Edition* 61 (2022): e202110429.

17. N. Meng, W. Liu, R. Jiang, et al., "Fundamentals, Advances and Perspectives of Piezocatalysis: A Marriage of Solid-State Physics and Catalytic Chemistry," *Progress in Materials Science* 138 (2023): 101161.

18. M. Wang, B. Wang, F. Huang, and Z. Lin, "Enabling PIEZOpotential in PIEZOelectric Semiconductors for Enhanced Catalytic Activities," *Angewandte Chemie International Edition* 58 (2019): 7526.

19. Z. Chen, M. Pan, C. Cheng, J. Luo, and X. Deng, "Water Disinfection: Advances in Photocatalysis and Piezo/Triboelectric Catalysis With Progressively Enhanced Energy Utilization," *SusMat* 4, no. 5 (2024): e232.

20. T. Jiang, Y. Wang, C. Cai, C. Nie, H. Peng, and Z. Ao, "Piezocatalysis for Water Treatment: Mechanisms, Recent Advances, and Future Prospects," *Environmental Science and Ecotechnology* 23 (2025): 100495.

21. N. Hoàng Ly, S. J. Son, H. Kamyab, Y. Vasseghian, and S.-W. Joo, "Dual-Function Piezo-Photocatalytic Systems for Sustainable Hydrogen Evolution and Environmental Remediation," *Advanced Science* 12, no. 46 (2025): e13811.

22. M. Zhang, S. Nie, T. Cheng, et al., "Enhancing the Macroscopic Polarization of CdS for Piezo-Photocatalytic Water Splitting," *Nano Energy* 90 (2021): 106635.

23. M. Song, S. Yang, H. Peng, et al., "Linkage Engineered the Donor–Acceptor Motifs of Poly(heptazine imide) for Enhancing the Piezo-Photocatalytic Nitrogen Fixation," *Nano Energy* 116 (2023): 108784.

24. J. Yuan, W. Feng, Y. Zhang, et al., "Unraveling Synergistic Effect of Defects and Piezoelectric Field in Breakthrough Piezo-Photocatalytic N_2 Reduction," *Advanced Materials* 36 (2024): e2303845.

25. C. Bi, H. Xu, G. Zhou, et al., "Lattice Energy Transfer From Homo-Crystalline Substitution for Enhanced Piezo-Photocatalytic CO_2 Conversion," *Chemical Engineering Journal* 501 (2024): 157345.

26. A. Verma and Y.-P. Fu, "Recent Developments in Piezo-Photocatalytic CO_2 Reduction: Concepts, Mechanism, and Advances," *Dalton Transactions* 53 (2024): 4890.

27. S. Mansingh, N. Priyadarshini, J. Panda, et al., "Recent Advancement in Piezopolarization Induced Photocatalytic H_2O_2 Production: Fundamentals, Theoretical Insights, and Future Endeavors," *Energy & Fuels* 38 (2024): 5632.

28. L. Zhao, M. Xu, S. Yang, Z. Zhu, J. Qi, and F. Meng, "Production of Hydrogen Peroxide by Piezocatalytic Processes: Mechanisms, Recent Advances, and Prospects," *ACS Sustainable Chemistry & Engineering* 13 (2025): 8853.

29. Y. Wang, X. Wen, Y. Jia, et al., "Piezo-Catalysis for Nondestructive Tooth Whitening," *Nature Communications* 11 (2020): 1328.

30. M. Ran, H. Xu, Y. Bao, Y. Zhang, J. Zhang, and M. Xing, "Selective Production of CO From Organic Pollutants by Coupling Piezocatalysis and Advanced Oxidation Processes," *Angewandte Chemie—International Edition* 62 (2023): e202303728.

31. J. Liu, W. Qi, M. Xu, T. Thomas, S. Liu, and M. Yang, "Piezocatalytic Techniques in Environmental Remediation," *Angewandte Chemie International Edition* 62 (2023): e202213927.

32. W. Qi, Y. Fu, E. Liu, et al., "Advancements and Opportunities in Piezo-(Photo)Catalytic Synthesis of Value-Added Chemicals," *EES Catalysis* 2 (2024): 884.

33. K. S. Suslick, "Sonochemistry," *Science* 247 (1990): 1439.

34. H. You, Z. Wu, L. Zhang, et al., "Harvesting the Vibration Energy of $BiFeO_3$ Nanosheets for Hydrogen Evolution," *Angewandte Chemie International edition* 58 (2019): 11779.

35. K. Tran, S. A. Tawfik, and M. J. Spencer, "Restoring Piezoelectric Properties in 2D Zinc Oxide Nanosheets by Surface Modifications: Implications for Piezoelectric Nanogenerators," *ACS Applied Nano Materials* 6 (2023): 14767.

36. M. Ritter, K. Maćkosz, J. Garemark, et al., "Piezoelectric and Photoconductive Zinc Oxide–Wood Hybrids Obtained by Atomic Layer Deposition," *ACS Nano* 19 (2025): 15161.

37. M. Ran, B. Du, W. Liu, et al., "Dynamic Defects Boost In-Situ H_2O_2 Piezocatalysis for Water Cleanup," *Proceedings of the National Academy of Sciences of the United States of America* 121 (2024): e2317435121.

38. X. Pan, X. Yang, M. Yu, et al., "2D MXenes Polar Catalysts for Multi-Renewable Energy Harvesting Applications," *Nature Communications* 14 (2023): 4183.

39. H. Gong, Y. Zhang, J. Ye, et al., "Retrievable Hierarchically Porous Ferroelectric Ceramics for "Greening" the Piezo-Catalysis Process," *Advanced Functional Materials* 34 (2024): 2311091.

40. C. Zhang, D. Lei, C. Xie, X. Hang, C. He, and H.-L. Jiang, "Piezo-Photocatalysis Over Metal–Organic Frameworks: Promoting Photocatalytic Activity by Piezoelectric Effect," *Advanced Materials* 33 (2021): e2106308.

41. M. Fu, J. Luo, B. Shi, et al., "Promoting Piezocatalytic H_2O_2 Production in Pure Water by Loading Metal-Organic Cage-Modified Gold Nanoparticles on Graphitic Carbon Nitride," *Angewandte Chemie International Edition* 63 (2024): e202316346.

42. L. Guan, Z. Li, K. Wang, et al., "Bottom-up Synthesis of Piezoelectric Covalent Triazine-Based Nanotube for Hydrogen Peroxide Production From Water and Air," *Angewandte Chemie International Edition* 64 (2025): e202419867.

43. C. Wang, C. Hu, F. Chen, T. Ma, Y. Zhang, and H. Huang, "Design Strategies and Effect Comparisons Toward Efficient Piezocatalytic System," *Nano Energy* 107 (2023): 108093.

44. K. Kubota, Y. Pang, A. Miura, and H. Ito, "Redox Reactions of Small Organic Molecules Using Ball Milling and Piezoelectric Materials," *Science* 366 (2019): 1500.

45. Y. Saito, H. Takao, T. Tani, et al., "Lead-Free Piezoceramics," *Nature* 432 (2004): 84.

46. W. Jiang, H. Zhu, J. Yang, et al., "Integration of Single-Atom Catalyst With Z -Scheme Heterojunction for Cascade Charge Transfer Enabling Highly Efficient Piezo-Photocatalysis," *Advanced science* 10 (2023): e2303448.

47. Y. Wang, Y. Xu, S. Dong, et al., "Ultrasonic Activation of Inert Poly(tetrafluoroethylene) Enables Piezocatalytic Generation of Reactive Oxygen Species," *Nature communications* 12 (2021): 3508.

48. W. Wang, Y. Shi, W. Chai, et al., "H-Bonded Organic Frameworks as Ultrasound-Programmable Delivery Platform," *Nature* 638 (2025): 401.

49. Z. Li, Z. Dong, Z. Zhang, et al., "Covalent Organic Frameworks for Boosting H_2O_2 Photosynthesis via the Synergy of Multiple Charge Transfer Channels and Polarized Field," *Angewandte Chemie International Edition* 64 (2025): e202420218.

50. P. Wang, S. Fan, X. Li, J. Duan, and D. Zhang, "Modulating the Molecular Structure of Graphitic Carbon Nitride for Identifying the Impact of the Piezoelectric Effect on Photocatalytic H_2O_2 Production," *ACS Catalysis* 13 (2023): 9515.

51. Y. Shao, C. Liu, H. Ma, et al., "Piezocatalytic Performance Difference of Graphitic Carbon Nitride (g-C_3N_4) Derived From Different Precursors," *Chemical Physics Letters* 801 (2022): 139748.

52. M. Xu, S. Yang, C. Guo, D. DuBois, S. Chen, and F. Meng, "Bubble-Triggered Piezocatalytic Generation of Hydrogen Peroxide by Copper

Nanosheets-Modified Polyvinylidene Fluoride Films for Organic Pollutant Degradation and Water Disinfection," *Water Research* 283 (2025): 123865.

53. L. Zhou, L. Meng, H. Jia, et al., "Recent Advances in Piezocatalysts for Dye Degradation," *Advanced Sustainable Systems* 8, no. 8 (2024): 2300652.

54. K. V. A. Birkelbach, S. Brettschneider, P. Huth, M. A. Liauw, and R. Palkovits, "*submitted* (Preprint: 10.26434/chemrxiv-2025-86f9b)," (2025).

55. A. Iemhoff, M. Vennewald, and R. Palkovits, "Single-Atom Catalysts on Covalent Triazine Frameworks: At the Crossroad Between Homogeneous and Heterogeneous Catalysis," *Angewandte Chemie—International Edition* 62 (2023): e202212015.

56. J. Artz, "Covalent Triazine-Based Frameworks—Tailor-Made Catalysts and Catalyst Supports for Molecular and Nanoparticulate Species," *Chemcatchem* 10 (2018): 1753.

57. K. V. A. Birkelbach, H. Hartmann, A. Besmehn, et al., "Enabling the Terpyridine Ligand Motif for Ir-Based Solid Molecular Catalysts," *EES Catalysis* 3, no. 4 (2025): 701–711.

58. Q. Wang, C. Yu, H. Long, Y. Du, Y. Jin, and W. Zhang, "Solution-Phase Dynamic Assembly of Permanently Interlocked Aryleneethynylene Cages Through Alkyne Metathesis," *Angewandte Chemie—International Edition* 54 (2015): 7550.

59. E. Tabrizian, A. Amoozadeh, S. Rahmani, E. Imanifar, S. Azhari, and M. Malmir, "One-Pot, Solvent-Free and Efficient Synthesis of 2,4,6-triarylpyridines Catalyzed by Nano-Titania-Supported Sulfonic Acid as a Novel Heterogeneous Nanocatalyst," *Chinese Chemical Letters* 26 (2015): 1278.

60. N. Davari, J. V. Pasikhani, C. L. Bianchi, V. Yargeau, and D. C. Boffito, "Recent Progress on Ti-Based Piezo-Photocatalysts for Wastewater Treatment," *Current Opinion in Chemical Engineering* 47 (2025): 101090.

61. Y. Nosaka and A. Y. Nosaka, "Generation and Detection of Reactive Oxygen Species in Photocatalysis," *Chemical Reviews* 117 (2017): 11302.

62. Y. Wang, Z. Yi, J. Guo, et al., "In Vivo Ultrasound-induced Luminescence Molecular Imaging," *Nature Photonics* 18 (2024): 334.

63. Y. Jiang, J. Liang, F. Zhuo, et al., "Unveiling Mechanically Driven Catalytic Processes: Beyond Piezocatalysis to Synergetic Effects," *ACS Nano* 19 (2025): 18037.

64. P. Makuła, M. Pacia, and W. Macyk, "How to Correctly Determine the Band Gap Energy of Modified Semiconductor Photocatalysts Based on UV–Vis Spectra," *The Journal of Physical Chemistry Letters* 9 (2018): 6814–6817.

65. J. Tauc, "Electronic Properties of Amorphous Materials: Changes are considered which occur when the long-range order typical for crystals disappears," *Science* 158, no. 3808 (1967): 1543–1543, https://doi.org/10.1126/science.158.3808.1543.

66. R. Raciti, R. Bahariqushchi, C. Summonte, A. Aydinli, A. Terrasi, and S. Mirabella, "Optical Bandgap of Semiconductor Nanostructures: Methods for Experimental Data Analysis," *Journal of Applied Physics* 121, no. 23 (2017): 234304, https://doi.org/10.1063/1.4986436.

67. F. Urbach, "The Long-Wavelength Edge of Photographic Sensitivity and of the Electronic Absorption of Solid," *Physical Review* 92, no. 5 (1953), https://doi.org/10.1103/PhysRev.92.1324.

68. P. Garcia-Munoz, L. Valenzuela, D. Wegstein, et al., "Photocatalytic Synthesis of Hydrogen Peroxide From Molecular Oxygen and Water," *Topics in current chemistry* 381 (2023): 15.

69. H. Cheng, J. Cheng, L. Wang, and H. Xu, "Reaction Pathways Toward Sustainable Photosynthesis of Hydrogen Peroxide by Polymer Photocatalysts," *Chemistry of Materials* 34 (2022): 4259.

70. D. Meyerstein, "Re-Examining Fenton and Fenton-Like Reactions," *Nature Reviews Chemistry* 5 (2021): 595.

71. J. P. Kehrer, "The Haber–Weiss Reaction and Mechanisms of Toxicity," *Toxicology* 43 (2000): 43–50.

72. A. L. Andrady, A. M. Heikkilä, K. K. Pandey, et al., "Effects of UV Radiation on Natural and Synthetic Materials," *Photochemical & Photobiological Sciences* 22 (2023): 1177.

73. T. Chen, J. Xie, and P. Gao, "Ultraviolet Photocatalytic Degradation of Perovskite Solar Cells: Progress, Challenges, and Strategies," *Advanced Energy and Sustainability Research* 3 (2022): 2100218, https://doi.org/10.1002/aesr.202100218.

74. T. G. McKenzie, F. Karimi, M. Ashokkumar, and G. G. Qiao, "Ultrasound and Sonochemistry for Radical Polymerization: Sound Synthesis," *Chemistry–A European Journal* 25 (2019): 5372.

75. M. Sillanpää, T.-D. Pham, and R. A. Shrestha, *Ultrasound Technology in Green Chemistry* (Springer, 2011).

76. B. Niemczewski, "Observations of Water Cavitation Intensity Under Practical Ultrasonic Cleaning Conditions," *Ultrasonics sonochemistry* 14 (2007): 13.

77. M. Binnie, R. T. K. Napp, J. W. D. Aily, and F. G. H. Ammitt, "Cavitation," *Journal of Fluid Mechanics* 54, (1972): 189–191.

78. E. Vlaisavljevich, K.-W. Lin, A. Maxwell, et al., "Effects of Ultrasound Frequency and Tissue Stiffness on the Histotripsy Intrinsic Threshold for Cavitation," *Ultrasound in Medicine & Biology* 41 (2015): 1651.

79. V. S. Bachu, J. Kedda, I. Suk, J. J. Green, and B. Tyler, "High-Intensity Focused Ultrasound: A Review of Mechanisms and Clinical Applications," *Annals of Biomedical Engineering* 49 (2021): 1975.

Supporting Information

Additional supporting information can be found online in the Supporting Information section.

Supporting File 1: anie71770-sup-0001-SuppMat.docx.